Atlas Based AAM and SVM Model for Fully Automatic MRI Prostate Segmentation

Ruida Cheng, Baris Turkbey, William Gandler, Harsh K. Agarwal, Vijay P. Shah, Alexandra Bokinsky, Evan McCreedy, Shijun Wang, Sandeep Sankineni, Marcelino Bernardo, Thomas Pohida, Peter Choyke, Matthew J. McAuliffe

***Abstract*— Automatic prostate segmentation in MR images is a challenging task due to inter-patient prostate shape and texture variability, and the lack of a clear prostate boundary. We propose a supervised learning framework that combines the atlas based AAM and SVM model to achieve a relatively high segmentation result of the prostate boundary. The performance of the segmentation is evaluated with cross validation on 40 MR image datasets, yielding an average segmentation accuracy near 90%.**

I. Introduction

Segmentation of T2 weighted (T2w) prostate MRI images is important for automated prostate cancer diagnosis and therapy planning. Current literature on MRI prostate segmentation focuses on atlas-, shape- and machine learning-based models. Klein et al. [1] proposed an automatic segmentation method based on atlas matching with non-rigid registration. Yin et al. [2] proposed an automated segmentation model based on normalized gradient field cross-correlation for initialization, and graph search based framework for refinement. Ghose et al. [3] proposed to use texture feature from approximation coefficients of a Haar wavelet transform for propagation of a shape, and Active Appearance Model (AAM) to segment the prostate. Toth et al. [4] extended the traditional AAM model to include intensity and gradient information, and used level-set to capture the shape statistical model information with a multi-feature landmark free framework. A registration scheme is used to locate the coarser prostate region. Habes et al. [5] proposed support vector machines (SVM) based automatic MRI prostate segmentation by using combined three-dimensional (axial, sagittal, coronal) image texture features.

In this paper, a novel combination of partial idea from above approaches [1-5] is used to create a new non-parametric atlas based method to automatically segment the prostate in 3D T2w MRI images. To build the atlas, we extract 2D slices from 3D prostate images, and apply AAM training and SVM classifier on a 2D slice-by-slice basis. To fully automatically segment a new 3D prostate MRI image, we propagate an automatic segmentation pipeline to each 2D slice to generate the final prostate contour. The method utilizes an adaptive AAM model to initialize the coarser prostate contour, followed by SVM to refine the prostate boundary. The two proposed models are 2D based.

Ruida Cheng, William Gandler, Evan McCreedy, Thomas Pohida, Matthew J. McAuliffe are with the Image Science Laboratory, Center of Information Technology, National Institutes of Health, Bethesda, MD. (e-mail: ruida@mail.nih.gov, tel: (301) 496-5363).

Baris Turkbey, Marcelino Bernardo, Harsh K Agarwal, Sandeep Sankineni, Peter Choyke are with the Molecular Imaging Program, National Cancer Institute, Bethesda, MD.

Alexandra Bokinsky is with Geometric Tools, Inc, Chapel Hill, NC.

Shijun Wang is with the Imaging Biomarker and CAD Laboratory, NIH Clinical Center, Bethesda, MD.

Harsh K Agarwal is with Philips Research NA Briarcliff Manor, NY.

Vijay P. Shah is with VirtualScopics, Inc, Rochester, NY.

II. Method

A. Atlas Based AAM Segmentation

The atlas based AAM training is 2D slice based as Figure 1 with the algorithm propagating from slice 1 to slice n. The algorithm extracts a 2D slice to create a volume of interest (VOI) based atlas. An exhaustive search algorithm subdivides the atlas into smaller groups with a similar shape measure. The similarity measure follows the work of Arkin et al. [6] to categorize VOI shapes with the shapes' turning functions. The L_2 metric on the turning functions is used to compute the shape resemblance. After forming the smaller group, the search algorithm marks the relevant images and VOIs as visited, and iteratively searches the data in the atlas, terminating when no more similarity shapes can be found.

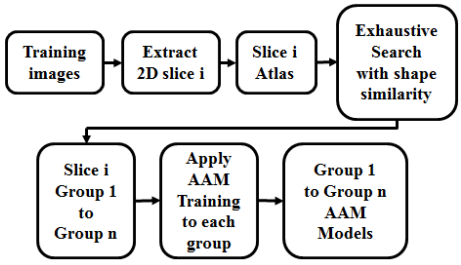

Figure 1. Atlas based AAM training

Each smaller group performs AAM training independently. We follow the work of Stegmann et al. [7] and Cootes et al. [8] to create the AAM model with the images and VOIs inside the smaller group. The AAM algorithm contains two stages: the AAM model creation and the AAM model fitting. The AAM model performs statistical analysis with the shape, the texture, and combined appearance of shape and texture. The images and VOIs inside the smaller group form the training set. The shape vectors $x^i = (x_1^i, \dots, x_n^i,\ y_1^i, \dots,\ y_n^i),\ i = 1 \dots N$ of the N training images are aligned using Procrustes Analysis [8]. The 2D prostate images are warped to the mean shape $\bar{x}$ and normalized, yielding the texture vector g^i. By applying principal component analysis (PCA) to the normalized data, linear models are obtained for both shape, $x = \bar{x} + P_s b_s$, and texture, $g = \bar{g} + P_g b_g$, where $\bar{x}, \bar{g}$ are the mean vectors, P_s, P_g are sets of orthogonal modes of variation, such as

eigenvectors resulting from PCA, and b_s, b_g are sets of model parameters. To combine the correlations between the shape and texture variations, a third PCA is applied using the following concatenated vector,

$$\mathrm{b} = \begin{pmatrix} W_s\, b_s \\ b_g \end{pmatrix} = \begin{pmatrix} W_s P_s^T (x - \bar{x}) \\ P_g^T (g - \bar{g}) \end{pmatrix} \qquad (1)$$

where W_s is a diagonal scaling matrix derived from the value range of the eigenvalues of the shape and texture eigenspaces. This yields the final combined linear model $b = P_c c$, where $P_c = \left(P_{cs}^T, P_{cg}^T\right)^T$, c is the vector of appearance parameters controlling both the shape and texture. AAM is trained to update model and pose with first order Taylor approximation [7]. After the AAM model has been trained, we choose the first sample image as the pivot image for atlas based image searching in the AAM search step. One additional adaptive step is to check the number of principal parameters of AAM PCA model after training. If the number is less than 2, we discard the group since the single parameter always introduces a twist contour in the fitting step. We add a conservative check to reduce segmentation errors.

The atlas based AAM fitting is also 2D based as shown in Figure 2.

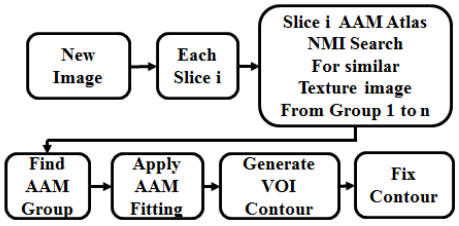

Figure 2. Atlas based AAM fitting

For the new image, a texture similarity measure (NMI) for each 2D slice is performed with all the smaller groups inside the AAM atlas. Normalized mutual information (NMI) is used to compute the image similarity between each 2D slice and the pivot sample image of the AAM model group. When the closest texture sample image is found, the corresponding AAM model is invoked, and AAM model fitting is applied to generate the prostate contour. AAM model searching is unstable due to the local minima, and sometimes can result in a twisted contour. To overcome this drawback, we apply a shape based similarity measure [6] to filter out those contours and replace them with consecutive neighboring contours.

The AAM search is an optimization problem in which the algorithm minimizes the difference between a target image $I_{image}(p)$ and one synthesized image $I_{model}(p)$ by the appearance model. The search for the model parameter p is guided by using the knowledge about how the difference images correlate with the parameter displacements, which is obtained from training. For each search step, the current image difference between the model texture $g_m(p)$ and the sampled image $g_s(p)$ is defined as,

$$r(p) = g_s(p) - g_m(p) \qquad (2)$$

To locate the best match between model and image, the search procedure minimizes sum of square error,

$$\Delta = \frac{1}{2} r(p)^T r(p) \qquad (3)$$

Building the derivative of (3) with p set to zero gives,

$$\delta p = -R\, r(p) \qquad (4)$$

where

$$R = \left(\frac{\delta r^T}{\delta p}\frac{\delta r}{\delta p}\right)^{-1}\frac{\delta r^T}{\delta p} = \left(\frac{\delta r}{\delta p}\right)^{Pseudo} \qquad (5)$$

R is the Pseudo inverse. Iterative refinement method is used to optimize the search [8]. During the search, each iteration updates the model parameter $p_{next} = p_{current} + k\delta p$, with pose parameters k (scale, translate, rotate). Evaluate the current error, $E_{current} = |g_s - g_m|^2$. Perturb k to produce $E_{next}(k) < E_{current}$. Set $p_{current}$ to p_{next}, and continue the next iteration. If no improvement can be found, the algorithm converges and $p_{current}$ is the best estimate for the model parameters.

B. Atlas based SVM Segmentation

Atlas based AAM segmentation results depend on how many images and VOIs are trained, and the number of pose configurations (rotation, translation, scale) applied during AAM model searching. In some cases the resulting contour looks promising. In most of the cases, the resulting contour still segments the prostate in coarser levels. To improve the AAM segmentation result, we apply the atlas SVM machine learning based algorithm to refine the prostate boundary. Figure 3 shows the flowchart of the proposed training method pipeline. To create the atlas based SVM model, we randomly select 20 images as the trained images, which represent the clear prostate boundary. We extract 2D slices from each 3D image, and apply the supervised SVM training to each 2D slice. A coherence enhanced diffusion (CED) filter removes the speckle noise in the 2D image before training. To build the SVM model, we establish two stages training. First, we individually train the non-prostate regions, which are the colored regions shown in Figure 3. We utilize MIPAV [15] semi-manual contouring tool to manually segment all the non-prostate regions for the 20 images.

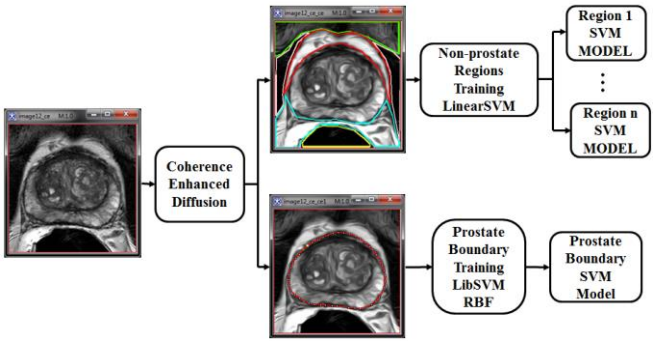

Figure 3. Atlas based SVM models training

The training phases collect texture priors of non-prostate regions and classify pixels for different sub-regions around the prostate by using the Hurst index [9] and Haralick [10] features. For each sub-region, a pixel is labeled by 1 or -1 to represent the class membership belonging to the VOI drawn region or not. Then, the sub-regions are trained

independently of each other to form a group of locally trained SVM models. Next, we train the prostate boundary. We extract the Hurst index and Haralick features on the points along the boundary line for a single class, and train the boundary SVM model. Non-prostate SVM modeled sub-regions, boundary SVM model, and 2D slice itself form a single unit of 2D slice based SVM trained model. The 2D slice is the pivot sample image, which will be used for searching texture images in the classification step. We decompose all the 20 images into 2D slices, and manually train the SVM model for each 2D slice. All the trained SVM models combine together to build the atlas based SVM model committee.

To construct the SVM based classifiers, we utilize different kernel functions to train the non-prostate sub-regions and prostate boundary. SVM is a supervised classifier based on statistical learning theory as proposed by Vapnik [11]. Due to the large pixel based feature space size, we employed the two-class (binary) SVM classifier with linear discriminate function to the non-prostate sub-regions. LibLinear [12] is used to speed up the performance. Given the training set, $\Omega = \{(x_1, y_1), (x_2, y_2), \ldots, (x_n, y_n)\}$, $x_i \in \mathcal{R}^p$ are independent feature vector of dimensionality p and $y_i \in \{1, -1\}^n$ are class labels for the binary classifier. We use linear kernel as the discriminate function,

$$K(x_i, x_j) = x_i^T x_j \qquad (6)$$

A detailed description of SVMs can be found in [11].

Traditional SVM prostate classifier specifies the region inside the prostate as +1, and region outside as -1. This approach is always error prone due to the high variability of the internal prostate anatomy structure. The non-prostate regions have low texture variation. Thus, we train the non-prostate regions with an intention to achieve robust classification of non-prostate regions with linear SVM.

For the prostate boundary training, we utilize the one-class classifier with non-linear Radial Basis (RBF) kernel function,

$$K(x_i, x_j) = \exp\left(-\gamma \|x_i - x_j\|^2\right), \ \gamma > 0 \qquad (7)$$

where γ is the kernel parameter and $\|x_i - x_j\|$ is the dissimilarity measure. The function returns $+1$ in a small region that captures the boundary training data points and -1 elsewhere. LibSVM [13] is used to train the boundary data. RBF kernel is a slow classifier. In the general case, 2D slice based prostate segmentation can take up more than 20 minutes to execute one non-linear based classification. In our case, we only train the prostate boundary points with smaller feature space size, significantly enhancing the RBF classification speed.

Atlas based SVM classification is demonstrated in Figure 4. With a new 3D prostate image, the segmentation pipeline propagates to each 2D slice. The algorithm applies the CED filter to remove the noise, and uses NMI to search the pivot sample images inside the SVM model atlas. When the closest image is found, the algorithm extracts features and invokes the corresponding SVM models to do classification. Binary mask images for the non-prostate region and prostate boundary are generated as the classification results, as shown in Figure 5.

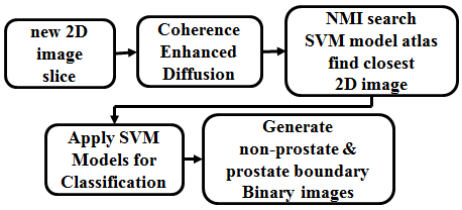

Figure 4. Atlas based SVM classification

AAM segmentation generates the coarser level contour in the 2D image. We use the contour as the initialization VOI, and copy it to non-prostate region and prostate boundary binary mask images. A narrow band algorithm searches the finer prostate boundary from the three images. Figure 5 shows the flowchart of the tracing pipeline.

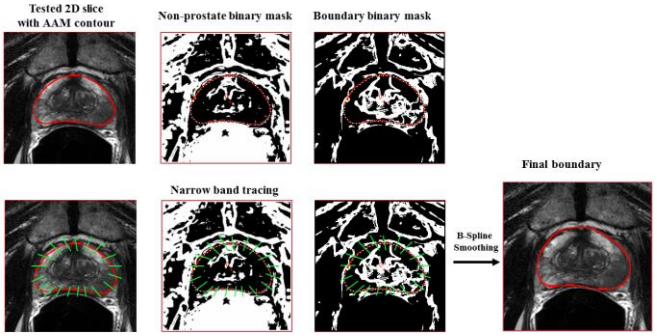

Figure 5. Narrow band tracing

The dynamic algorithm sequentially searches the initial VOI boundary points. For each boundary point, it traces the points within the narrow band region along the polar coordinate system α angle expansion line. The green lines in Figure 5 illustrate the searching path. From the tested 2D slice and the two binary mask images, the algorithm looks for the point that satisfies the following criterion as the ideal prostate boundary point: 1) the point has a high gradient magnitude change in the original 2D slice; 2) the point stands close to the binary masked boundary; 3) the point does not belong to the non-prostate region mask image. In some cases, not all the three conditions can be satisfied, and we use the current AAM segmented boundary point as the resulting search point. B-Spline interpolation applies to all the found ideal points to generate the final smooth prostate boundary.

III. Experiment and Results

The proposed fully automatic segmentation method is evaluated with 100 prostate 3D axial MR images as the base training set, and 40 new 3D axial MR images as the testing set. All the datasets were collected from different patients, and provided by National Cancer Institute, Molecular Imaging Branch. The MR images are obtained from a 3.0 T whole-body MRI system (Achieva, Philips Healthcare). T_2-weighted MR images of the entire prostate were obtained in axial planes at the scan resolution of 0.2734x0.2734x3.0 mm^3; field of view 140 mm; image slice dimension 512x512. The center of the prostate is the focal point for MRI scan. The experimental results are evaluated by comparing the

automatic segmentation with the expert manual segmentation. The expert manual segmentation is made by trained researchers and verified by a radiologist. These VOIs are considered as the ground truth of the evaluation.

The atlas based SVM model is built by randomly selecting 20 images from the training set as described in section B. The atlas based AAM model is built from the 100 MR images as described in section A. Leave-one-out cross validation is applied to the testing set to evaluate the segmentation performance. Basically, we pull out one image from the 40 images, train the rest images with the AAM model, and merge them with the base AAM model as a committee. Then, the fully automatic segmentation pipeline that combines the atlas based AAM+SVM model (method B) generates the prostate VOI contour from the new image. One additional test we do is to apply the atlas based AAM (method A) model alone to generate the contour. The experimental results are evaluated based on the previous work [14], for example, true positive (TP), false negative (FN), false positive (FP), and the VOIs volume. We also use the Dice Coefficient. Table 1 illustrates the average volume percent difference and average VOI overlapped region for both models: AAM standalone model and AAM+SVM guided model. Evaluation compares the automated and the manual segmentation results with the expert segmentation as the ground truth. The proposed method achieves 90% average segmentation accuracy for the TP overlapped region, and the average Dice similarity is 87%. The FP shows a relative high percent difference, which mostly comes from the over-interpolated slices near apex and base. The AAM+SVM combined model improves the TP accuracy 10% more than the AAM standalone model. Volume difference is measured with the whole segmented VOIs volume without trimming VOI contours at apex and base. Figure 6 demonstrates the visual segmentation results. The red contours present the automatic AAM+SVM model; the green contours present the manual segmentation.

	TP	***FN***	***FP***	***Dice***	***V-Diff***
AAM (method A)	82.85%	13.61%	16.45%	86.60%	-2.37%
AAM+SVM (method B)	91.2%	8.78%	19.25%	87.58%	8.38%

Table 1. Segmentation performance

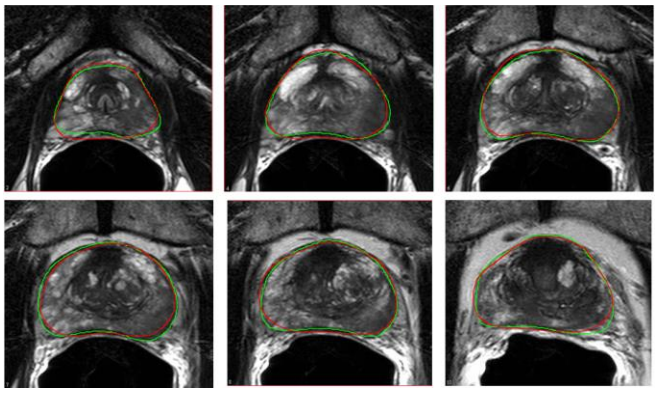

Figure 6. AAM+SVM model segmentation results

The traditional AAM standalone model requires large amount of images and VOIs to accurately capture shape variations [4]. Also, to train the AAM model with a large texture and shape variation dataset can be prone to errors. The smaller number of eigenvalues in the AAM PCA model suffers from the local minima in the AAM model searching step. We propose the atlas based AAM training with a smaller group to ensure that relatively similar images and VOI shapes can be trained with a higher number of eigenvalues in the PCA model. The exhaustive searching algorithm generates large amount of groups to capture the shape and texture variations. With contour fixing at the end of fitting, the atlas based AAM model can significantly reduce the segmentation errors. The atlas based SVM model utilizes the non-prostate regions and prostate boundary classifiers to ensure more stable prostate classification. To combine the two, AAM generates the initial coarser VOI contour. Then, SVM stretches the initial contour toward the correct prostate boundary location with the narrow band tracing algorithm. With the limited 100 MRI prostate images given as the training set, our proposed method yields promising segmentation results. Our method relies heavily on AAM to initialize the contour. When the initial contour is far from the narrow band reaching ranges, the proposed method fails. The proposed models (AAM, AAM+SVM) are all implemented in Java under MIPAV [15] software, which is open source and can be obtained from http://mipav.cit.nih.gov.

IV. Conclusion

A novel atlas based method for automatic MRI prostate segmentation was presented in the paper. We combine the AAM and SVM model with an atlas based approach to tolerate errors from either model alone, and still generate relatively accurate segmentation results. The proposed method utilizes adaptive atlas based AAM model that reduce the AAM segmentation errors. The atlas based SVM non-prostate regions and prostate boundary classifier ensures more reliable classification around the prostate. The segmentation results were fine-tuned with the combination of atlas based AAM and SVM model with a dynamic narrow band tracing algorithm. While the prostate segmentation is improved with better TP, FN and Dice coefficient, further work is required to improve the FP and volume difference.

References

[1] S. Klein, U.A. van der Heide, I. M. Lipps, M. V. Vulpen, M. Staring, and J. P. W. Pluim, "Automatic segmentation of the prostate in 3D MR images by atlas matching using localized mutual information," Medical Physics, vol. 35, no. 4, pp. 1407-1417, 2008.

[2] Y. Yin, S. V. Fotin, S. Periaswamy, J. Kunz, H. Haldankar, N. Muradyan, F. Cornud, B. Turkbey, P. Choyke, "Fully automated prostate segmentation in 3D MR based on normalized gradient fields cross-correlation initialization and LOGISMOS refinement," Proc. SPIE 8314, 831406, 2012.

[3] S. Ghose, A. Oliver, R. Marti, X. Llado, J. Freixenet, J. C. Vilanava, F. Meriaudeau, "Texture guided active appearance model propogation for prostate segmentation," MICCAI workshop PCI, LNC, Springer, Vol. 6367, pp. 111-120, 2010.

[4] R. Toth, A. Madabhushi, "Multifeature landmark-free active appearance models: application to prostate MRI segmentation," IEEE Trans Med Imaging, (8): 1638-50, 2012.

[5] M. Habes, T. Schiller, C. Rosenberg, M. Burchardt, W. Hoffmann, "Automated prostate segmentation in whole-body MRI scans for epidemiological studies," Phys Med Biol, 58(17):5899-915, 2013.
[6] E. Arkin, L. Chew, D. Huttenlocher, K. Kedem, and J. Mitchell, "An efficiently computable metric for comparing polygonal shapes," IEEE Trans Patt Anal Mach Intell, 13(3), pp. 209-216, 1991.
[7] M. B. Stegmann, B. K. Ersboll, and R. Larsen, "FAME-A Flexible Appearance Modeling Environment", IEEE Trans. Med. Imag., 22(10):1319-1331, October, 2003.
[8] T. F. Cootes, G. J. Edwards, and C. J. Taylor, "Active appearance models", Proc. Eur. Conf. Comput. Vis. 2:484-498, 1998.
[9] C. Chen, J.S. Daponte, M.D. Fox, "Fractal feature analysis and classification in medical imaging", IEEE Trans. Med. Imag., Vol. 8, No. 2, pp. 133-142, June, 1989.
[10] D.A. Clausi, "An analysis of co-occurrence texture statistics as a function of grey level quantization", Canadian Journal of remote sensing, 28(1), 45-62, 2002.
[11] V. Vapnik*, The Nature of Statistical Learning Theory 2nd edition*, Springer-Verlag, 2000.
[12] R. E. Fan, K. W. Chang, C. J. Hsieh, X. R. Wang, and C. J. Lin, "LIBLINEAR: A library for large linear classification", Journal of Machine Learning Research, 1871-1874, Sep, 2008.
[13] C. C. Chang, C. J. Lin, "LIBSVM: a library for support vector machines," ACM Transactions on Intelligent Systems and Technology, 2:27:1—27:27, 2011.
[14] R. Cheng, B. Turkbey, J. Senseney, M. Bernardo, A. Bokinsky, W. Gandler, E. McCreedy, T. Pohida, P. Choyke, M. McAuliffe, "2D registration guide models for semi-automatic MRI prostate segmentation," Proc. SPIE 8669, Medical Imaging: Image Processing, 86692V, Mar, 2013.
[15] M. J. McAuliffe, F. M. Lalonde, D. McGarry, W. Gandler, K. Csaky, and B. L Trus, "Medical image processing, analysis, and visualization in clinical research," in 14th IEEE CBMS, Proceedings, pp. 381-386, 2001.